NMR and spin relaxation in systems with magnetic nanoparticles



2007 J. Phys.: Condens. Matter 19 076210

(http://iopscience.iop.org/0953-8984/19/7/076210)

IOP PUBLISHING JOURNAL OF PHYSICS: CONDENSED MATTER

J. Phys.: Condens. Matter **19** (2007) 076210 (10pp) doi:10.1088/0953-8984/19/7/076210

# NMR and spin relaxation in systems with magnetic nanoparticles

**N Noginova[1], T Weaver[1], M King[1], A B Bourlinos[2], E P Giannelis[3] and V A Atsarkin[4]**

[1] Norfolk State University, Centers for Materials Research, Norfolk, VA, USA
[2] Institute of Materials Science, NCSR Demokritos, Athens, Greece
[3] Cornell University, Ithaca, NY, USA
[4] Institute of Radio Engineering and Electronics RAS, Moscow, Russia

Received 10 October 2006, in final form 30 November 2006
Published 2 February 2007
Online at stacks.iop.org/JPhysCM/19/076210

**Abstract**

The $^1$H NMR spectra and spin dynamics of the host systems have been studied in liquid and solid suspensions of $\gamma$-$Fe_2O_3$ nanoparticles. Significant broadening of $^1$H NMR spectra and growing relaxation rates were observed with increased concentration of nanoparticles in the liquid systems, with the relation $T_1/T_2$ depending on the particular host. Solid systems demonstrate inhomogeneous broadening of the spectra and practically no dependence of $T_1$ upon the nanoparticle concentration. We explain the experimental results taking into account the predomination of self-diffusion as a source of the relaxation in liquid suspensions, and estimate effective parameters of relaxation in the systems under study.

(Some figures in this article are in colour only in the electronic version)

## 1. Introduction

Magnetic nanoparticles have shown great potential for many interesting applications in science, technology and biology, including magnetic resonance imaging (MRI) and medical hyperthermia. The effect of the magnetic nanoparticles on the nuclear spin relaxation of the host in liquid systems has been studied in a number of papers using the relaxometry technique [1–3]. Most of the experiments were performed in liquid (aqueous) solutions of $Fe_2O_3$ or Co nanoparticles and concentrated on moderate fields corresponding to the range of Larmor frequency $0.01 < f < 50$ Hz. The general theory describing the effect is based on the classical outer sphere paramagnetic relaxation model [4] by taking into account the high magnetization and magnetic anisotropy values of nanoparticles [3]. It was shown that the model qualitatively well describes the profiles of the field dependence of the longitudinal spin relaxation with a maximum in the range 1–30 MHz depending on the magnetic properties of the nanoparticles in a particular sample.

  

The specifics of NMR and spin relaxation at higher field (7 T) were studied in [5] in aqueous solutions of ionic ferrofluids with grains of ∼8 nm. It was shown that besides homogeneous broadening the NMR spectrum demonstrates non-homogeneous broadening as well, and could not be well described with only the outer sphere model. The broadening was ascribed to the effect of grain aggregates, which may have significant size and require special consideration.

To better understand the peculiarities of NMR and spin relaxation of nanoparticle systems, we conducted an experimental study of the dependence on concentration and temperature of suspensions with surface-modified maghemite nanoparticles in different liquid and solid hosts. In addition to clarification of the mechanisms of broadening and relaxation, the NMR and spin relaxation studies of magnetically diluted systems may provide information on the magnetic and dynamic behaviour of magnetic impurities as well, and serve as an independent method for nanoparticle characterization.

## 2. Experimental details

The experimental samples were prepared using a solvent-free ferrofluid containing surface-functionalized maghemite ($\gamma$-$Fe_2O_3$) nanoparticles of diameter $d \sim 5$ nm. Such a ferrofluid has been produced by attaching a corona of flexible chains onto maghemite nanoparticles. Specifically, the reaction of a positively charged organosilane ($(CH_3O)_3Si(CH_2)_3N^+(CH_3)(C_{10}H_{21})_2Cl^-$) with surface hydroxyl groups on the nanoparticles leads to a permanent covalent attachment to the surface and renders the nanoparticles positively charged. A counter anion is present to balance the charge leading to a hybrid nanoparticle salt. Sulfonate anions ($R(OCH_2CH_2)_7O(CH_2)_3SO_3^-$, R: $C_{13}$–$C_{15}$ alkyl chain) were used, yielding a liquid at room temperature with a nanoparticle content around 40 wt% [6]. From TEM images, the size distribution of the nanoparticles was found to be nearly log-normal, with a mean diameter of $d = 4.8$ nm and dispersion $\sigma = 0.15$.

The ferrofluid was characterized with the electron magnetic resonance (EMR) method, which revealed the saturated magnetization value of $M \sim 400$ emu ($4 \times 10^5$ A m$^{-1}$) and relatively small anisotropy field of ∼600 G [7]. The EMR and microscope data indicated that, along with individual nanoparticles, there are small aggregates formed through dipole–dipole interactions between nanoparticles [7].

To prepare experimental samples with different concentrations, the ferrofluid was dispersed in liquid (toluene and water) and solid polymer matrices. The polymer used was poly(styrene-co-butadiene-co-methyl methacrylate) (Aldrich #45, 751-5).

The weight contents of the ferrofluid in the samples are presented in table 1.

The nanoparticle concentration, $n$, is related to the weight content, $C\%$, of the ferrofluid as

$$n = \frac{0.4C\rho_{\text{host}}}{100V_0\rho_{\text{Fe}}}$$

where $V_0 = \pi d^3/6$ is the nanoparticle volume; $\rho_{\text{Fe}}$, and $\rho_{\text{host}}$ are the densities of $\gamma$-$Fe_2O_3$ and diamagnetic solvent correspondingly.

A Bruker Avance 300 NMR spectrometer was used in the experiments. The relaxation times $T_1$ were measured by the standard saturation–recovery technique. The echo technique was used to study spin–spin relaxation in the samples with non-homogeneous broadening. The duration of the $\pi/2$ pulse is about 8 $\mu$s. Variable temperature measurements were performed using a VT Bruker system.

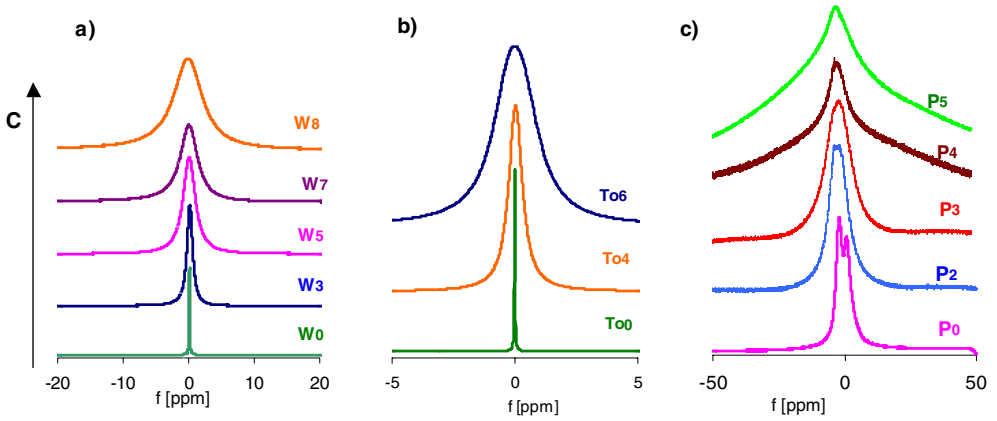


**Figure 1.** $^1$H spectra of water (a), toluene (b) and polymer (c) with different concentrations of $\gamma$-$Fe_2O_3$ nanoparticles. The toluene line shown in the figure corresponds to the $CH_3$ group. The samples are indicated in the graph; see table 1 for the corresponding concentrations.

**Table 1.** Concentrations of the nanoparticles in the samples under study. The concentrations are determined as the relative weight of the ferrofluid in the solution.

| Host:water | | Toluene | | Polymer | |
|---|---|---|---|---|---|
| Sample | $C$ (%) | Sample | $C$ (%) | Sample | $C$ (%) |
| $W_0$ | 0 | $To_0$ | 0 | $P_0$ | 0 |
| $W_1$ | 0.11 | $To_1$ | 0.03 | $P_1$ | 0.1 |
| $W_2$ | 0.2 | $To_2$ | 0.07 | $P_2$ | 0.2 |
| $W_3$ | 0.34 | $To_3$ | 0.13 | $P_3$ | 0.6 |
| $W_4$ | 0.43 | $To_4$ | 0.27 | $P_4$ | 1.1 |
| $W_5$ | 0.55 | $To_5$ | 0.33 | $P_5$ | 2.3 |
| $W_6$ | 0.64 | $To_6$ | 0.51 | | |
| $W_7$ | 1.1 | $To_7$ | 0.63 | | |
| $W_8$ | 2.7 | | | | |

## 3. Results

The spectra of the suspensions at different concentrations are presented in figure 1.

As one can see, the increase in nanoparticle concentration results in substantial broadening of the spectra in both solid and liquid systems. In the liquid systems the broadening is symmetrical and homogeneous up to high concentrations (2.7 wt%). The line can be well described with a Lorentzian line-shape. The opposite is seen in the solid solution, where the broadening has more complicated character. At least two components of a different width are observed in the concentrated samples, with the width of the broad component of the order of the spectral window of the spectrometer.

No echo beyond the free induced decay is observed in the liquid systems, indicating the homogeneous character of the broadening in toluene and water solutions. In this case, the relaxation rates $T_2^{-1}$ were determined from the spectral half-width from the fitting of the line with the Lorentzian shape.

The concentration dependence of the transverse relaxation rates in the liquid suspensions is shown in figure 2(a).

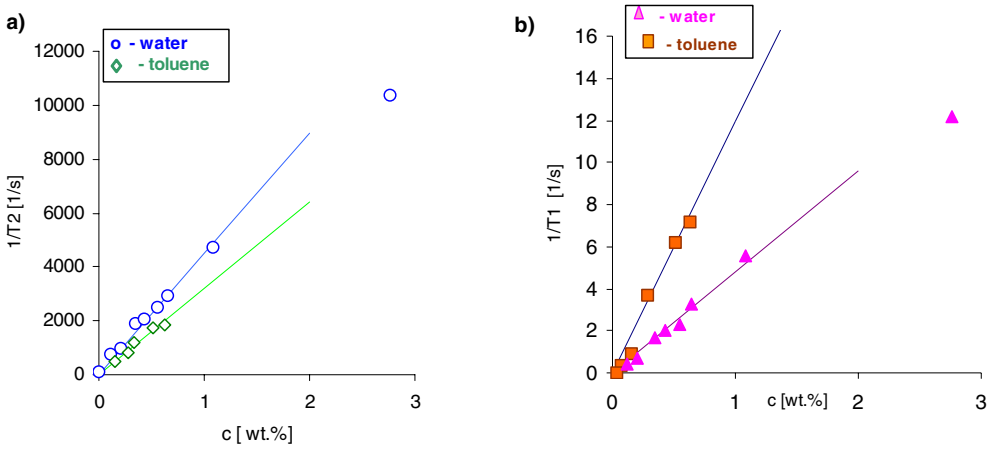


**Figure 2.** The spin relaxation rates of toluene and water protons in the ferrofluid suspensions. (a) $T_2^{-1}$. (b) $T_1^{-1}$.

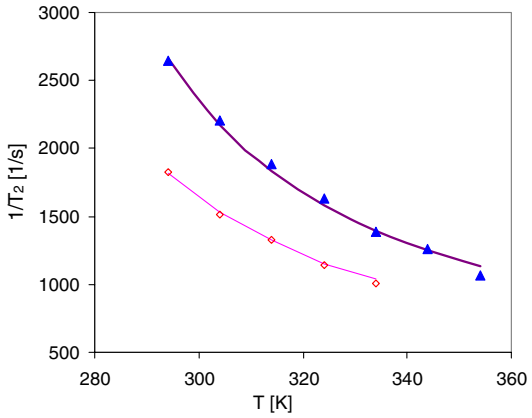


**Figure 3.** Temperature dependences of the transverse relaxation rates in water and toluene systems, sample $W_5$ (triangles) and sample $To_7$ (diamonds), correspondingly. Solid lines represent fitting with equation (3).

In both water and toluene samples, the transverse relaxation rate $T_2^{-1}$ demonstrates approximately linear growth with the increase in the ferrofluid concentration. The relaxation rates in water are slightly higher than the rates in toluene at the same concentrations.

The longitudinal relaxation rates in liquid systems, $T_1^{-1}$, grow with the concentration as well. Figure 2(b) presents the contribution to the rate associated with the nanoparticles estimated as $T_1^{-1} = T_{ex}^{-1} - T_o^{-1}$, where $T_{ex}$ is the time determined from the recovery dynamics, and $T_o$ corresponds to the solvent without nanoparticles (samples $W_0$ and $To_0$ with $T_1 = 3$ and 9 s correspondingly). As one can see, in similarity with the spin–spin relaxation rates, $T_1^{-1}$ grows linearly with increasing concentration, but in this case the slope of the concentration dependence $T_1^{-1}(C)$ in toluene is significantly higher than that in water.

The liquid systems demonstrate significant narrowing of the spectrum with heating; see figure 3.

In solid suspensions, the transverse relaxation times are determined through echo decay. The echo decay practically does not depend on the nanoparticle concentration; see figure 4.

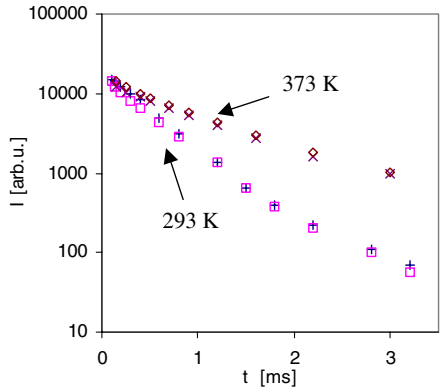


**Figure 4.** Echo decay in $Po_0$ at room temperature (crosses), 373 K (×), and in $Po_4$ at room temperature (squares) and 373 K (diamonds).

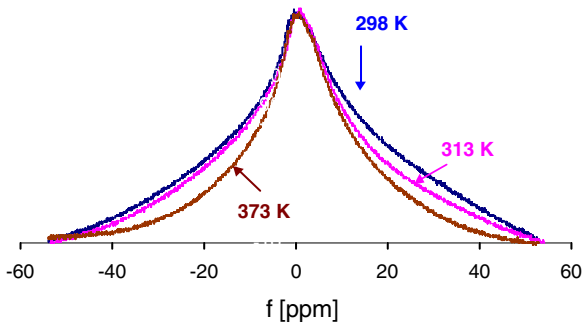


**Figure 5.** Spectra in $Po_4$ at different temperatures.

However, it depends on temperature, slowing down from $T_2 \sim 0.4$ to 1.2 ms with heating from 293 to 373 K.

Similarly, no visible changes were observed with increase in nanoparticle concentration for the spin–lattice relaxation ($T_1$ is ∼1.4 s at room temperature and slightly decreases with heating to 1.3 s at 373 K).

As one can see in figure 1(c), the spectrum in solid suspensions demonstrates strong non-homogeneous broadening. With heating, the shape of the spectrum changes, and the broad component narrows slightly; see figure 5.

We fitted the spectra of figure 5 as a sum of two components of Lorentzian shape, with the width and magnitude of components depending on temperature. The fitting parameters are shown in table 2, where $\Delta_1$ and $\Delta_2$ are half-widths of the components, and $A_1$ and $A_2$ are their amplitudes. From the fitting, the width of the narrow component is practically temperature independent while the width of the broad one decreases with increase in temperature; see figure 6.

## 4. Discussion

In systems with magnetic impurities, nuclear relaxation is related to dipole–dipole interactions between magnetic moments of the impurity and nuclear magnetic moments. The rates of the

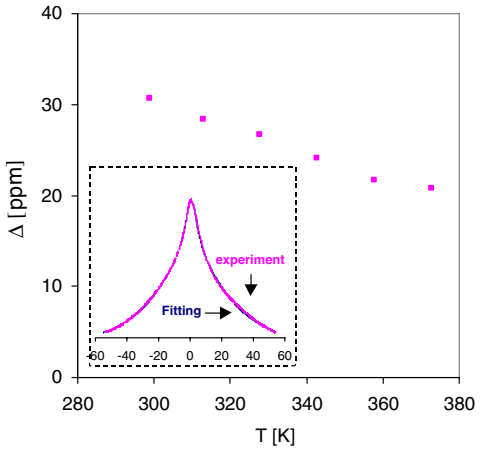


**Figure 6.** The dependence of the width of the broad component on temperature. The inset demonstrates an example of fitting by two Lorentzian lines.

**Table 2.** Fitting parameters for $P_4$.

| $T$ (K) | $\Delta_1$ (ppm) | $\Delta_2$ (ppm) | $A_1\Delta_1/A_2\Delta_2$ |
|---|---|---|---|
| 299 | 4.7 | 30.6 | 0.014 |
| 313 | 4.8 | 28.3 | 0.02 |
| 328 | 4.7 | 26.7 | 0.022 |
| 343 | 4.7 | 24 | 0.031 |
| 358 | 4.7 | 21.7 | 0.041 |
| 373 | 4.7 | 20.7 | 0.043 |

relaxation are determined by the magnitude and rate of random variation of local fields induced by magnetic impurities on host nuclei.

Here one can distinguish two mechanisms of nuclear relaxation. The first one is related to thermally induced fluctuations of the magnetic moment of the magnetic impurity; this mechanism can be observed in both liquid and solid systems with paramagnetic ions.

The other mechanism is associated with motion of the host molecules through a steady-state magnetic field that is non-uniform in space. This mechanism works for liquid systems only, and is determined by the self-diffusion of the host molecules, which has the characteristic time $\tau_D = R^2/D$, where $D$ is the diffusion constant, and $R$ is the effective radius of the nanoparticle.

In solid systems without any significant motion of the host molecules, only the mechanism related to the electron-spin fluctuations would play a role. However, according to our experiments with suspensions of $Fe_2O_3$ nanoparticles, no visible changes are observed in the relaxation kinetics and temperature dependence of the spectra in the polymer samples.

This situation is related to the high-spin polarization of nanoparticles with a relatively large magnetic moment, $\mu = MV_0 \sim 3\times10^{-17}$ emu ($3\times10^{-20}$ A m$^2$). The rate of nuclear relaxation caused by the fluctuating part of $\mu$ (denoted by $\Delta\mu_z$) is proportional to

$$\Delta\mu_z^2 = \langle\mu_z^2\rangle - \langle\mu_z\rangle^2 = \mu^2(1/\xi^2 - 1/sh^2\xi), \tag{1}$$

where $\mu_z$ is the projection of $\mu$ on the direction of the external field $\mathbf{H}$; $\xi = \mu H/kT$; and $\langle\cdots\rangle$ denotes thermal averaging. (The right-hand part of equation (1) is calculated analogously to

the derivation of the Langevin law for a high-spin particle.) For our samples at $T = 300$ K and $H = 70$ kOe, one has $\xi \sim 50$ and $\Delta\mu_z^2/\mu^2 = 4 \times 10^{-4}$. Thus, though local fields induced by nanoparticles are quite strong, as seen from the width of the non-homogeneously broadened spectra, the magnitudes of their temporal variations are relatively small. Estimating for our materials, for a proton situated, for example, 14 nm from the centre of the nanoparticle, the local field magnitude is up to 2.8 G (at 70 kG that corresponds to a frequency shift of 40 ppm from the central position) but its fluctuating part is only of 0.047 G. Protons situated closer to a nanoparticle would experience higher fluctuating fields, but also much higher steady-state fields, which shift their frequency far from the central frequency and make them unobservable in experiments. Due to the high gradients of the local magnetic fields, spin diffusion is not effective, and the spin relaxation kinetics of the majority of the observable protons in solid suspensions under study is determined by other sources (such as other paramagnetic impurities, hindered molecular motion, and inter-nuclear interactions) rather than nanoparticle-related ones.

In liquid systems, generally both mechanisms may play role. Fast-moving molecules experience variations in the magnetic field due to the thermal fluctuations and a spatial non-uniform field. The broadening of the spectra can have both homogeneous and non-homogeneous character depending on how fast the molecules are moving and how efficient the averaging of the local field is.

However, simple estimations predict strong domination of the diffusion-related mechanism for our liquid systems. In this case, the formulae for the relaxation rates [3, 4] can be simplified as

$$\frac{1}{T_1} = \frac{32\pi}{135}\gamma_I^2 \frac{n}{RD}[3J^A(\sqrt{2\omega_I}\tau_D)\langle\mu_z\rangle^2] \tag{2}$$

$$\frac{1}{T_2} = \frac{32\pi}{135}\gamma_I^2 \frac{n}{RD}\left[\frac{3}{2}J^A(\sqrt{2\omega_I}\tau_D) + 2J^A(0)\right]\langle\mu_z\rangle^2. \tag{3}$$

Here $\gamma_I$ is the gyromagnetic ratio of the proton, $n$ is the nanoparticle concentration per cm$^3$, $D$ is the self-diffusion constant of the solvent, $R$ is the effective radius associated with a magnetic nanoparticle, $\tau_D = R^2/D$, and $J^A(z)$ is the spectral density of the correlation function.

$$J^A(z) = \frac{1 + 5z/8 + z^2/8}{1 + z + z^2/2 + z^3/6 + z^4/81 + z^5/81 + z^6/648}. \tag{4}$$

Equations (2) and (3) predict a linear dependence of the relaxation rates, $T_1^{-1}$ and $T_2^{-1}$, on the nanoparticle concentration. This is observed in the experiment, see figure 2, for a broad range of nanoparticle concentration, with the exception of the highest concentration, which demonstrates slightly lower rates.

The observed narrowing of the NMR line in liquid suspensions with heating can be ascribed just to the temperature dependence of the diffusion coefficient. According to equation (3), $T_2^{-1}$ is approximately inversely proportional to $D$. Indeed, one can see that the temperature dependence of the transverse relaxation rate, figure 3, is well consistent with $D^{-1}(T)$ [8, 9], confirming the predominating role of the diffusion mechanism. To fit the observed relaxation rates quantitatively, other parameters entering the equations (2), (3) need to be fixed, the $R$ value being the most ambiguous of them.

The radius $R$ is associated with the distance at which a moving molecule experiences sharp changes in the magnetic field, induced by the nanoparticles. Commonly, $R$ is considered to be of about a nanoparticle size; however, it may be significantly larger. First, the organic surfactant on the surface of the nanoparticle would keep the solvent molecules at some distance. Second, $R$ can increase due to the aggregation of nanoparticles.

A way to estimate $R$ independently of other parameters is provided by the comparison of $T_1$ and $T_2$. Note that, according to equations (2) and (3), the ratio $T_2^{-1}/T_1^{-1}$ does not depend on the concentration or magnetic energy of a nanoparticles but is determined by the radius $R$ as

$$\frac{T_1}{T_2} = \frac{\frac{3}{2}J^A\left(\sqrt{2\omega_I}\tau_D\right) + 2J^A(0)}{\frac{3}{2}J^A\left(\sqrt{2\omega_I}\tau_D\right)} \approx \frac{2}{3J^A\left(R\sqrt{\frac{2\omega_I}{D}}\right)}. \tag{5}$$

Let us use $R$ as a fitting parameter and compare the predictions of the model with the experimental data, starting with room temperature. As an example, let us consider the toluene suspension $To_7$ with the concentration of the nanoparticles of 0.63 wt%, demonstrating the ratio $T_1/T_2 = 253$, and the aqueous system $W_5$ with $C = 0.55$ wt% and $T_1/T_2 = 1114$. Note that the nanoparticle concentration is nearly the same in both samples, $n = 6.7 \times 10^{15}$ cm$^{-3}$. From equation (5), the effective radius can be estimated as 9 and 15 nm for the samples $To_7$ and $W_5$ correspondingly. Evidently, these values considerably exceed the nanoparticle radius, if even the organic corona is taken into account. The discrepancy might be caused by the failure of the theory initially intended for a description of nuclear relaxation via paramagnetic molecules which are much smaller in size than the nanoparticles. Another explanation might be related to the aggregation of particles due to their dipole–dipole interaction. Some evidence for this effect was reported in [7].

Let us assume that $R$ is the average size of aggregates, and substitute into equations (2) and (3) $n = n_0(R_0/R)^3/F$, where $n_0 = 6.7 \times 10^{15}$ cm$^{-3}$ is the concentration of the nanoparticles, $R_0 = 2.5$ nm is the radius of an individual maghemite grain, and $F < 1$ is the effective 'filling' factor introduced to take into account the non-magnetic part of the aggregate, $1 - F$. As a magnetic moment we consider $\mu' = F\mu(R/R_0)^3$, which corresponds to the moment of the aggregate. Now we will fit the experimental $T_2^{-1}$ values using $F$ as a fitting parameter and retaining the $R$ values obtained above from the $T_1/T_2$ fitting. We found that the experimental values for the relaxation rates in the toluene sample, $T_2^{-1} = 1.8 \times 10^3$ s$^{-1}$ and $T_1^{-1} = 7.2$ s$^{-1}$, can be fitted with $R = 9$ nm and $F = 0.1$. For the water suspension, the experimental $T_2^{-1} = 2.5 \times 10^3$ s$^{-1}$ and $T_1^{-1} = 2.3$ s$^{-1}$ can be fitted with $R = 15$ nm and $F = 0.05$. According to this approach, the average numbers of maghemite particles in a cluster are about of 5 and 10 in toluene and water respectively.

The solid curves in figure 3 show the fitting obtained with these parameters and using the $D(T)$ dependence for water [8] and toluene [9]. A very good agreement is evident.

The obtained $F$ values are also in a good agreement with the volume fraction of $Fe_2O_3$ in the dense ferrofluid ($\sim$0.1). The difference between water and toluene may be attributed to differing penetration abilities of the $H_2O$ and $C_7H_8$ molecules in the area filled by the organic chains attached to the particle surface, as well as to various stereometry of these chains in water and toluene. Further studies, especially with particles of various size, would be quite useful to clarify this issue.

Let us now discuss the results obtained for the polymer systems. We suggest that the broad component of the NMR line (figures 5 and 6) is dominated by dipole–dipole interaction of nuclear spins with randomly distributed magnetic nanoparticles. According to Anderson's statistical theory [10], at a low enough concentration of magnetic impurities, the NMR line shape is Lorentzian with a half-width of

$$\Delta_L = \gamma\frac{8\pi^2}{9\sqrt{3}}\langle\mu_z\rangle n. \tag{6}$$

This theory, however, was developed originally in the high-temperature approximation, provided that the electron spin polarization $P = \langle\mu_z\rangle/\mu \ll 1$. At higher $P$, an

antisymmetric (dispersion-like) component arises, leading to an asymmetric distortion of the line shape [11, 12]. Both the generalized statistical theory [11] and the moment calculation [12] show that the magnitude of this distortion is proportional to $P(1 - P^2)$. This expression attains its maximum near $P \sim 0.6$ and becomes negligible in our case ($P = 0.98$), so we can use Anderson's theory, equation (6). Estimating for our case of $\mu \sim 3 \times 10^{-17}$ emu and $n \sim 10^{16}$ cm$^{-3}$ at 1.1 wt%, one gets $\Delta_L = 21$ ppm, which is reasonably close to the half-width of the broad component. The width of the narrow component is of the order of that observed in the pure polymer sample. The two-component spectra may indicate that in our solutions the distribution of the nanoparticles in not completely random. Note that the ratio of the areas under the narrow and broad lines, $A_1\Delta_1/A_2\Delta_2$, shown in table 2 is relatively small, ∼2–5%. The narrow line could be the contribution of the areas in the sample which are relatively free from the nanoparticles.

The spin relaxation in polystyrene-based polymers is determined by a number of various processes, including flips of the phenyl rings, oscillations of chains, or direct relaxation with the participation of oxygen [13, 14]. The increase in the relaxation time $T_2$ around 340 K is typical, indicating the large-scale motion due to approaching the glass transition ($T_g \approx 373$ K for the polymer used). The cooperative large-scale motion would cause partial averaging of the fields induced by nanoparticles, resulting in some narrowing of the spectra, as was observed in the experiment. Further investigation of this phenomenon might provide a deeper insight into molecular kinetics in polymers.

In conclusion, $^1$H NMR spectra and spin dynamics of host systems have been studied in liquid and solid suspensions of $\gamma$-$Fe_2O_3$ nanoparticles with respect to the dependence on the nanoparticle concentration and temperature. Significant homogeneous broadening of $^1$H NMR spectra and growing relaxation rates were observed with the increased concentration of nanoparticles in the liquid systems, with the relation $T_1/T_2$ depending on the particular host. Narrowing of the spectra is observed with increase in temperature. The experimental results obtained in liquid suspensions can be explained by a standard outer-sphere model with the predomination of self-diffusion as a source of the relaxation and modification of the effective radius to account for the formation of the aggregates. The solid systems demonstrate inhomogeneous broadening of the spectra and practically no dependence of spin relaxation times upon the nanoparticle concentration. The results have been discussed taking into account the large polarization of the superparamagnetic nanoparticles.

## Acknowledgments

The work was partially supported by National Science Foundation (NSF) CREST Project HRD-9805059, NSF PREM Grant No DMR-0611430, RFBR Grant 05-02-16371, and Program P-03 for Basic Research of the Russian Academy of Sciences.

## References

[1] Roch A, Gillis P, Ouakssim A and Miller R N 1999 *J. Magn. Magn. Mater.* **201** 77–9
[2] Bautista M C, Bomati-Miguel O, Zhao X, Morales M P, Gonzales-Carreno T, Perez de Alejo R, Roiz-Cabello J and Veintemillas-Verdaguer S 2004 *Nanotechnology* **15** S154–9
[3] Roch A, Muller R N and Gillis P 1999 *J. Chem. Phys.* **110** 5403–11
[4] Toth E, Helm L and Merbach A E *Relaxivity of MRI Contrast Agents* (*Springer Topics in Current Chemistry*) (Berlin: Springer) pp 61–101
[5] Gonzalez C E, Pusiol D J, Neto A M F, Rama M, Bourdon A and Bee A 2003 *J. Phys. Chem.* B **107** 646–50
[6] Bourlinos A B, Herrera R, Chalkias N, Jiang D D, Zhang Q, Archer L A and Giannelis E P 2005 *Adv. Mater.* **17** 234

[7] Noginova N, Chen F, Weaver T, Giannelis E P, Bourlinos A B and Atsarkin V A 2006 *Preprint* cond-mat/0610383
[8] Mahoney M W and Jorgensen W L 2001 *J. Chem. Phys.* **114** 363–6
[9] Harris K R, Alexander J J, Goscinska T, Malhotra R, Woolf L A and Dymond J H 1993 *Mol. Phys.* **78** 235–48
[10] Anderson P W 1951 *C. R. Acad. Sci. Paris* **82** 342
Abragam A 1961 *The Principles of Nuclear Magnetism* (Oxford: Clarendon) chapter 4
[11] Dzheparov F S and Henner E K 1989 *Phys. Status Solidi* b **151** 663
[12] Abragam A, Chapellier M, Jaquinot J-F and Goldman M 1973 *J. Magn. Reson.* **10** 322
Abragam A and Goldman M 1982 *Nuclear Magnetism: Order and Disorder* (Oxford: Clarendon) chapter 5
[13] Froix M F, Williams D J and Goedde A O 1976 *Macromolecules* **9** 354–9
[14] Pschorn U, Rossler E, Sillescu H, Kaufmann S, Schaefer D and Spiess H W 1991 *Macromolecules* **24** 398–402